JGR Oceans

RESEARCH ARTICLE
10.1029/2019JC015882

Key Points:
- AUV deployment to East Antarctic ice shelf finds cold ocean conditions with deep bathymetric access
- Melt rate estimates and observations from an integrated survey show evidence of weak basal melting
- We posit that dense cold waters produced in nearby polynyas block access of MCDW and reduce melting

Supporting Information:
- Supporting Information S1

Correspondence to:
D. E. Gwyther,
david.gwyther@gmail.com

Citation:
Gwyther, D. E., Spain, E. A., King, P., Guihen, D., Williams, G. D., Evans, E., et al. (2020). Cold ocean cavity and weak basal melting of the Sørsdal ice shelf revealed by surveys using autonomous platforms. *Journal of Geophysical Research: Oceans*, *125*, e2019JC015882. https://doi.org/10.1029/2019JC015882

Received 17 NOV 2019
Accepted 19 MAY 2020
Accepted article online 23 MAY 2020

Cold Ocean Cavity and Weak Basal Melting of the Sørsdal Ice Shelf Revealed by Surveys Using Autonomous Platforms

David E. Gwyther[1], Erica A. Spain[1], Peter King[2], Damien Guihen[1], Guy D. Williams[1,3], Eleri Evans[1,3], Sue Cook[1,3], Ole Richter[1], Benjamin K. Galton-Fenzi[3,4], and Richard Coleman[1,3]

[1]Institute for Marine and Antarctic Studies, University of Tasmania, Hobart, Tasmania, Australia, [2]Australian Maritime College, University of Tasmania, Launceston, Tasmania, Australia, [3]Antarctic Climate & Ecosystems Cooperative Research Centre, University of Tasmania, Hobart, Tasmania, Australia, [4]Australian Antarctic Division, Kingston, Tasmania, Australia

Abstract Basal melting of ice shelves is inherently difficult to quantify through direct observations, yet it is a critical factor controlling Antarctic mass balance and global sea-level rise. While much research attention is paid to larger ice shelves and those experiencing the most rapid change, many smaller, unstudied ice shelves offer valuable insights. Here, we investigate the oceanographic conditions and melting beneath the Sørsdal ice shelf, East Antarctica. We present results from the 2018/2019 Sørsdal deployment of the University of Tasmania's autonomous underwater vehicle *nupiri muka*. Oceanography adjacent to and beneath the ice shelf front shows a cold and relatively saline environment dominated by Winter Water and Dense Shelf Water, while bathymetry measurements show a deep (~1,200 m) trough running into the ice shelf cavity. Two multiyear deployments of Autonomous Phase-sensitive Radar Echo Sounders on the surface of the ice shelf show weak melt rates (average of 1.6 and 2.3 m yr^{-1}) with low temporal variability. These observations are supported by numerical ocean model and satellite estimates of melting. We speculate that the presence of a ~825 m thick (350 m to at least 1,175 m) homogeneous layer of cold, dense water blocks access from warmer waters that intrude into Prydz Bay from offshore, resulting in weak melt rates. However, the newly identified trough means that the ice shelf is vulnerable to any decrease in polynya activity that allows warm water to enter the cavity. This could lead to increased basal melting and mass loss through this sector of Antarctica.

Plain Language Summary Ice shelves, the floating extensions of Antarctic glaciers, play a key role in retarding the flow of the ice sheet toward the ocean. Enhanced ocean-driven melting beneath these ice shelves can reduce this "buttressing" effect and increase the flow of the ice sheet into the ocean, leading to sea-level rise. We present the results from a first-time deployment of an autonomous underwater vehicle (AUV) to the Sørsdal ice shelf in East Antarctica. We found cold and salty water present beneath the ice shelf with a deep seafloor trough at the entrance to the ice shelf, indicative of a cold ocean environment with low melt rates. We also present results from surface-deployed radar instruments, numerical modeling, and remote sensing techniques, which confirm weak melting is occurring beneath this ice shelf. Though many studies document the presence of warm water in the region, we posit that this cold and salty water blocks warm water incursions in front of and into the cavity, maintaining the relatively weak melt rates. However, this process may change in the future, allowing entry of warmer water and increasing melting and sea-level contribution from this part of Antarctica.

1. Introduction

Ocean-driven melting at the base of ice shelves is the main contributor to mass loss from the Antarctic Ice Sheet (Liu et al., 2015). Ice shelves provide a buttressing backstress on the glaciers that drain the Antarctic Ice Sheet. A reduction in backstress can lead to glacial acceleration and increased contribution to mean sea level. Estimates of Antarctic mass loss in the recent period (2011–2017) range from 137 ± 25 gt yr^{-1} (Schröder et al., 2019) to 178 ± 23 gt yr^{-1} (Sasgen et al., 2019), bringing the total sea-level contribution from 1979–2017 to 13.9 ± 2.0 mm (Rignot et al., 2019). However, these rates have uncertainties that are magnified

when projected into the future, due to the incomplete understanding of dynamic ice processes (Church et al., 2013) such as the Marine Ice Sheet and Marine Ice Cliff Instabilities (DeConto & Pollard, 2016; Edwards et al., 2019). Detection and attribution of change is also made difficult by intrinsic, interannual, and decadal variability in oceanic and atmospheric forcing, which can obscure trends (Gwyther et al., 2018; Jenkins et al., 2018).

Increased heat flux to the base of ice shelves under a warming climate has been shown to increase basal melting, for example, in the Amundsen Sea (Arneborg et al., 2012; Dutrieux et al., 2014; Paolo et al., 2018). The delivery of heat to ice shelves is influenced by a variety of factors. Bathymetry of the continental shelf and troughs cross-cutting the shelf break can promote access of warmer off-shelf water masses (e.g., St-Laurent et al., 2013; Walker et al., 2013), while atmospheric interactions modify on-shelf waters, producing dense, cold water masses that can also produce melting (e.g., Nicholls et al., 2003). The under-ice cavity shape and bathymetry will have an impact on ocean circulation and hence on the spatial distribution of melting and freezing (Holland et al., 2008). On a smaller scale, tides (Gwyther et al., 2016; Mueller et al., 2012) and basal roughness (Gwyther et al., 2015) will also impact the magnitude and spatial pattern of melting. However, melting is not constrained to deeper ice. The frontal band (within 1–10 km of the calving front) of the Ross Ice Shelf has been shown to have melt rates an order of magnitude higher than the shelf-wide mean (Stewart et al., 2019). This is hypothesized to be due to inflow of solar-heated surface waters from the adjacent polynya, which is potentially facilitated by the formation of a freshwater wedge with poleward steepening of isopycnals (Malyarenko et al., 2019). The frontal band of many ice shelves is known to be important for providing a region of passive shelf ice, which can be lost with little impact on the dynamical state of the remaining ice shelf; loss of ice beyond the threshold of this passive ice can lead to reduction in buttressing and possible ice shelf collapse (Fürst et al., 2016). As a result, increased basal melt in the frontal band could have negative impacts on shelf stability (in the case of no passive shelf ice) or precondition the shelf to have a reduced passive ice buffer (in the case of passive ice in the frontal band).

Our efforts to better quantify basal melting are largely frustrated by the lack of cavity geometry (the ice draft and bathymetry), due to the extreme inaccessibility of these regions. Shipborne oceanography must negotiate hazardous and changing sea ice conditions, while on-ice shelf work, such as borehole moorings and seismic surveys, are logistically complex and are constrained by safety considerations. The answer may lie with autonomous underwater vehicles (AUVs).

AUVs are submersible robotic platforms with the capability to operate independently of direct human control. They can be configured with a wide variety of instruments, with oceanographic conductivity -temperature-depth (CTD) probes (Collar & McPhail, 1995) and seabed mapping (Wynn et al., 2014) being common types. Since their inception, the exploration of the cryosphere has been a motivating force behind the development and deployment of AUV capability. A number of AUV missions have been conducted underneath Arctic and Antarctic sea ice, mapping seabed (Crees et al., 2010), ecosystems (Brierley et al., 2002), and ice draft (Williams et al., 2015). Prior to 2019, AUVs have been used to investigate ocean properties within only two ice shelf cavities, Fimbul Ice Shelf (Nicholls et al., 2006; Nicholls et al., 2008) and Pine Island Glacier (Dutrieux et al., 2014; Jenkins et al., 2010; Kimura et al., 2016). As autonomy and support technology develops, the number of polar-capable AUVs will surely increase.

The navigation and safe maneuvering of AUVs is a complex problem. This is perhaps most evident under ice shelves, where the overhead environment and uncharted hazards for safe navigation pose distinct risks to the survival of the vehicle (Brito et al., 2010). The risk becomes acceptable when balanced against the reward of acquiring critical data that cannot be otherwise obtained, or when it is too dangerous or costly to send human operators. Vehicles operating in such environments rely on careful sensing of collision risks and make use of technologies such as inertial navigation, Doppler velocity logging, and beacon homing to determine their position while underwater. Onboard logic enables the vehicle to autonomously follow a predetermined mission path, while being flexible enough to make changes as operational and environmental circumstances dictate.

We present results from the first deployment of an AUV beneath an East Antarctic ice shelf. We show oceanography, bathymetry, and ice topography measurements of the region adjacent to and beneath the Sørsdal ice shelf. Our survey characterizes the oceanographic conditions that influence the ice shelf. New modeling and observational estimates of basal melting are presented and compared with satellite-based estimates. We hypothesize that basal melting below the Sørsdal ice shelf is low (a few meters per year) and

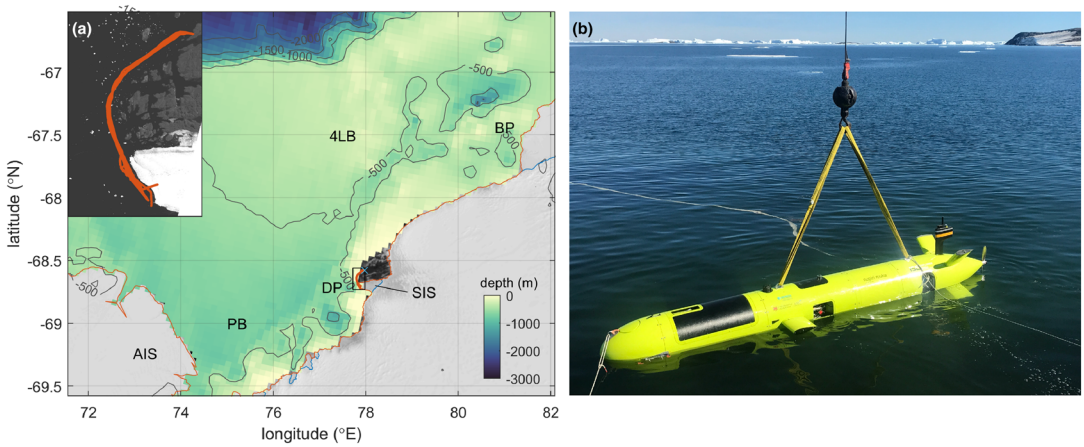

Figure 1. (a) The study region along the Ingrid Christiansen Coast is shown with bathymetry contours from IBCSO (Arndt et al., 2013). Key regions are labeled, including Four Ladies Bank (4LB), Barrier Polynya (BP), Davis Polynya (DP), Prydz Bay (PB), the Amery Ice Shelf (AIS), and the Sørsdal ice shelf (SIS). A blue cross shows the location of Davis Station, and orange lines show mission tracks. The small black box shows the extent of the inset (top left corner). The Sørsdal ice shelf region is shown in the inset, with orange lines showing tracks for all missions during deployment. Basemap images from MODIS. (b) The 6.5-m-long AUV *nupiri muka* lowered from the wharf at Davis Station. Photo: Glenn Johnstone.

that the low magnitude of melting is driven by cold oceanographic conditions. This study provides new insight into the unknown state of ocean-ice shelf interactions along this East Antarctic stretch of the Princess Elizabeth Land coastline.

2. Region and Methods

2.1. Sørsdal Glacier Ice Shelf Region

The Sørsdal Glacier flows westward from the Ingrid Christiansen Coast of Princess Elizabeth Land into Prydz Bay, a large embayment in the Indian Ocean sector of Antarctica (Figure 1). The floating extension of this glacier, which we refer to as the Sørsdal ice shelf (78.0°E, 68.7°S), is a ~5- to 8-km-wide by 20-km-long ice shelf located nearby to Davis Station (Australia) in East Antarctica. The Sørsdal ice shelf lies ~150 km east of the Amery Ice Shelf (AIS), the third largest ice shelf, on the eastern edge of Prydz Bay. The AIS has traditionally been thought of as being in approximate mass balance (e.g., King et al., 2009), due to the stable oceanographic regime with limited warm water access and most basal melting being driven by cold, denser water masses (Herraiz-Borreguero et al., 2015). There is, however, a net mass loss trend becoming apparent for the Amery drainage basin and Princess Elizabeth Land, estimated to have commenced in ~2012 (Schröder et al., 2019). Multiple recurring latent heat polynyas or intense sea ice formation regions (Massom et al., 1998), such as the Barrier, Davis, Mackenzie, and Cape Darnley polynyas, occur in the Prydz Bay region. These polynyas modify water properties through brine rejection from sea ice, which forms Dense Shelf Water (DSW). The Sørsdal ice shelf is situated immediately landward of the Davis Polynya and in relatively close proximity to the Barrier Polynya. The role of the Sørsdal in a region dominated by continental shelf and air-sea processes is unknown.

The ocean circulation in Prydz Bay is particularly important for explaining ice-ocean interactions along this coastline. The region is defined by a large clockwise gyre; the Prydz Bay Gyre forms in the deeper Amery Depression and is separated from shallower bathymetry to the west (Fram Bank and Cape Darnley) and the east (Four Ladies Bank). A narrow Antarctic Coastal Current (ACoC), driven by offshore and easterly winds, flows westwards near to the coast (Smith et al., 1984). Intrusion of Modified Circumpolar Deep Water (MCDW) occurs over Four Ladies Bank and eventually flows into the Prydz Bay Gyre and the AIS cavity (Galton-Fenzi et al., 2012; Liu et al., 2018). This MCDW is an important factor in driving basal melting of the AIS (Herraiz-Borreguero et al., 2015). This large MCDW water mass is present in eastern Prydz Bay, over the Four Ladies Bank and near to Davis Station. It is present at the near-surface and intermediate depths, from 250–450 m in eastern Prydz Bay and deeper 500–600 m closer to the AIS (Williams et al., 2016). The western side of Prydz Bay is dominated by Ice Shelf Water (ISW) flowing out from below the AIS. ISW is released by basal melting, typically at depth, and is characterized by temperatures below the surface freezing point.

2.2. AUV *nupiri muka* and Sørsdal Campaign

From October 2018 to March 2019, University of Tasmania and Australian Antarctic Division scientists and engineers deployed the AUV *nupiri muka* to Davis Station with the goal of proof-of-operation testing in a sub-ice shelf environment. *nupiri muka* is a 7-m-long, 1,600 kg AUV built by International Submarine Engineering in Vancouver, Canada. Capable of diving to 5,000 m, this AUV carries a comprehensive payload of acoustic instruments, in addition to two CTD probes and magnetometer. Deployment of *nupiri muka* was from shore by way of a modified boat trailer and available plant machinery at the Davis Station boat ramp. The transit to the Sørsdal calving front, a distance of ~18 km, took on average 2.5 hr, leaving 3 hr on station for operations.

The primary acoustic payload is a combined acoustic Doppler current profiler (ADCP) system, which synchronously collects side-scan intensity imagery and three-dimensional (3-D) bathymetry along a swath. In addition, a low-frequency subbottom profiler sonar collects echo intensity from subsurface layering. For the under-ice missions, the penetrative sonar was oriented upward to capture the basal surface of the ice. This low-frequency (4–24 kHz) and high-power (202 dB referenced at 1 μPa at 1 m) sonar can extract surface returns to a range in excess of 800 m, though horizontal resolution degrades quickly due to the 15° beam angular width. Ice draft is extracted by taking the maximal return intensity for each ping. Each return is then corrected for AUV motion of pitch, roll, heading, and depth.

While primary mission objectives were engineering and capability focused, deployments were designed to capture useful scientific data over the nine missions, of which two included incursions beneath the Sørsdal ice shelf. The staged nature of the planned missions meant that the first mission was conducted directly offshore of Davis Station, while the following six missions were conducted in the deep water in front of the ice shelf (Figure 1 inset). These missions, conducted between 20 January and 7 February 2019, measured temperature, salinity, and water currents along the calving front. The last phase of the mission consisted of two missions (3 and 7 February 2019) beneath the ice shelf, with successively longer distances traveled beneath the ice front.

2.3. Estimating Basal Melt

A numerical ocean model based on the Regional Ocean Modeling System (ROMS) framework was run for the Sørsdal ice shelf region and included modifications for ice/ocean thermodynamics and mechanical pressure, following Dinniman et al. (2007). This model, using similar configuration options, has been previously applied to several Antarctic ice shelves, such as the Mertz Glacier (Cougnon et al., 2013, 2017), Totten Glacier (Gwyther et al., 2014, 2018), Ross Ice Shelf (Jendersie et al., 2018), and the AIS (Galton-Fenzi et al., 2012). The model domain extended from 74.8°E to 80.8°E and 66.9°S to 69.5°S and was discretized on a polar stereographic grid with a uniform 2 km horizontal resolution (see supporting information Figure S1). The vertical terrain-following coordinate had 31 vertical layers with a sigmoidal layer distribution to provide higher vertical resolution at the surface and bottom regions.

Autonomous Phase-sensitive Radar Echo Sounder (APRES) instruments are a lightweight and low-power autonomous radar system designed by the British Antarctic Survey and University College London for long-term field deployment (Nicholls et al., 2015). The radar uses the frequency-modulated continuous wave technique, in which a tone sweeps from 200 to 400 MHz over a period of 1 s to form a chirp. Each APRES was set up to emit a burst every 2 hr, with a burst consisting of 30 chirps. For each burst, the chirps were averaged and the ice thickness was calculated automatically using an amplitude threshold to detect the ice base. Instruments were installed at two locations on the Sørsdal ice shelf from 2017 to 2018, Site s02 at 78.10°E, 68.71°S and Site s04 at 78.21°E, 68.71°S. Data quality is good, but performance is reduced when liquid water is present, leading to gaps in the data record during the Austral summer.

To ensure the effects of tidal flexure on ice thickness were removed, time series of data from both sites were filtered with a fifth-order Butterworth low-pass filter with cutoff frequency equivalent to 1 week. The time series were then corrected for long-term mean internal thickness change from vertical strain in the ice column, as estimated by tracking motion of internal reflectors (Nicholls et al., 2015). Both sites are in a blue ice zone (Hui et al., 2014); therefore, firn compaction does not need to be accounted for. Quality control was performed to remove data with erroneously high thickness change (principally this occurs during summer in the presence of liquid water) and is caused by change in the shape of the basal peak. Further details are given in the supporting information.

Satellite-based estimates of melt rate were calculated with two different techniques. First, we calculate two estimates of mean mass loss by using a flux gate method. Flux across the ice shelf grounding line is differenced from the flux across the calving front of the ice shelf, where the grounding line position is taken from both Bedmap2 and MEaSUREsv2, and the coastline data are taken from MEaSUREsv2. In all estimates, snow accumulation is removed (Arthern et al., 2006). The Sørsdal Glacier region is known to experience surface melting during summer, and so the surface accumulation product used (which does not capture this surface melting) will likely lead to an overestimation in melt rates. Ice thickness along both the grounding line and coastline is taken from Bedmap2. However, due to the poor representation of the floating ice shelf in the thickness data set, particularly near the coastline, this component is calculated from surface elevation, which is converted to thickness by assuming hydrostatic equilibrium with $\rho_{\text{water}} = 1{,}027\ \text{kg m}^{-3}$ and $\rho_{\text{ice}} = 917\ \text{kg m}^{-3}$. The second method used for estimating the basal mass loss was by considering the volume divergence of flow across the ice shelf. The change in ice shelf thickness with time is $\frac{\partial H}{\partial t} = \nabla\cdot(\mathbf{u}H)+\dot{M}_s+\dot{M}_b$, where $\mathbf{u}$ is the 3-D velocity field, $\dot{M}_s$ is the surface mass change in time, and $\dot{M}_b$ is the basal mass change. We assume that for a small, relatively stable ice shelf such as the Sørsdal ice shelf $\frac{\partial H}{\partial t} = 0$. H is calculated from both the Bedmap2 data set (Fretwell et al., 2013) and the Reference Elevation Map of Antarctica (REMA Howat et al., 2019). For the case of both Bedmap2 and REMA, surface elevation is converted to ice thickness by assuming hydrostatic equilibrium, with $\rho_{\text{water}} = 1{,}027\ \text{kg m}^{-3}$ and $\rho_{\text{ice}} = 917\ \text{kg m}^{-3}$. We assume the full 3-D velocity field is well represented by the surface velocity, which we derive from the MEaSUREsv2 data set (Mouginot et al., 2017). However, the results from the volume divergence method are hindered by the quality and resolution of their constituent components, and hence, we use these data with caution. It is presented in the supporting information for completeness.

3. Results

Collectively, the multitude of smaller ice shelves potentially contribute a substantial amount to the total mass loss of Antarctica. However, these smaller ice shelves often remain unstudied, principally due to the greater interest in larger ice shelves and those that are obviously displaying significant change. The region beneath and adjacent to the Sørsdal ice shelf was chosen as the target for engineering trials of *nupiri muka* mainly due to proximity to Davis Station. However, this presents a prime opportunity to investigate one such smaller ice shelf with an array of observation and modeling techniques. We present first-time oceanographic measurements from the onboard CTD (with all references to salinity on the Practical Salinity Scale) and ADCP, as well as sonar measurements of bathymetric and ice shelf topographic features. Oceanography results are further split into conditions in front of the ice shelf and conditions measured during incursions beneath the ice shelf. These observations are compared to modeling and observation-based estimates of basal melt to characterize the oceanographic environment adjacent to and beneath the Sørsdal ice shelf.

3.1. Oceanography at the Sørsdal Ice Shelf

Temperature and salinity in front of the ice shelf vary with depth (Figures 2a and 2b). Near-surface temperatures are relatively warm (~ -0.4°C) and fresh (33–34.25). The top 125 m is relatively isothermal with stratification being controlled by salinity. The warm temperatures and low salinity indicated that the top layer is a summer mixed layer (SML) and represents water that has been heated by the atmosphere and the Sun and contains fresher water from melted sea ice and icebergs. From the bottom of the SML to approximately 350 m, a thermocline shows mixing of the summer waters with a distinctly different water mass below. This thermocline water mass ranges from −0.4°C with salinity 34.2 to ~ -1.8°C with salinity ~34.5 and is most likely Winter Water (WW), which represents the remnants of wintertime convection. From the bottom of the thermocline at ~350 m to the very deepest sampled location (1,175 m), observations show a mostly homogeneous structure of cold and relatively salty Shelf Water, with DSW present at the bottom (−1.88°C with salinity >34.5).

The mean depth of the ice draft at the calving front is 300 m (dashed orange line in Figures 2a and 2b), which is derived from the satellite elevation product REMA, assuming hydrostatic equilibrium to calculate draft from surface elevation. This means that the warmer SML does not flow directly underneath the calving front, unless some process steepens the isopycnals toward the ice front. No freshwater lens was observed at the beginning of dives, which were ~500 m from the ice front. This suggests that a freshwater wedge, as suggested by Malyarenko et al. (2019), was not acting to steepen isopycnals at the ice front and allow access

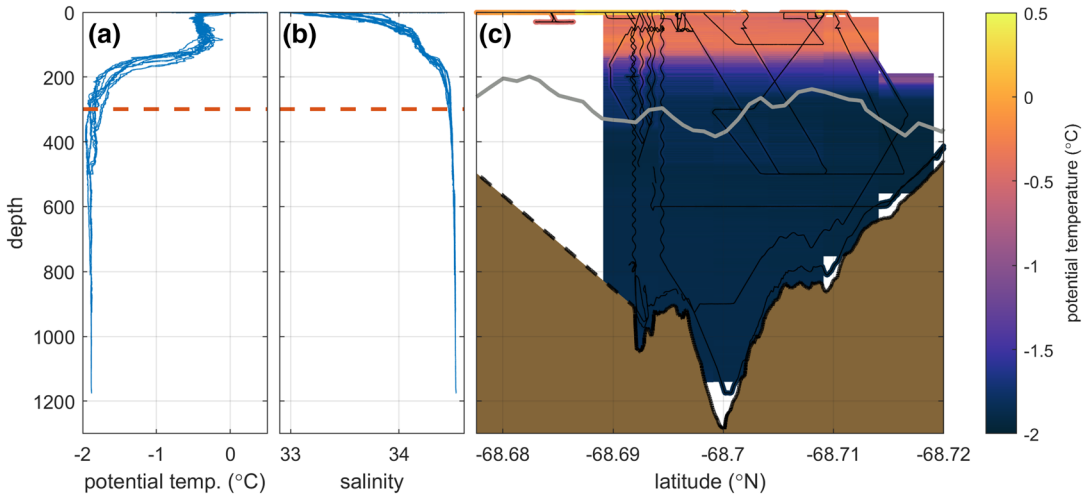

Figure 2. Oceanography observations at the Sørsdal ice shelf front. (a) Potential temperature measurements with depth and (b) salinity measurements with depth. In both (a) and (b), the dashed orange line marks the mean ice draft as derived from the satellite elevation product REMA (Howat et al., 2019). (c) A meridional composite of all potential temperature data showing the interpolated temperature field, the estimated ice draft at the calving front from REMA (gray line), and the bathymetry (brown patch, with solid bounding line for observations from ADCP and dashed bounding line for linear interpolation between ADCP data). In (c), thin black lines show the paths of AUV dives and measurements.

of SML into the cavity. However, a full diagnosis of the potential for baroclinic flow leading to shallow-ice melting would require more observations.

By comparing the data collected with a meridional view looking into the Sørsdal ice shelf cavity, we can appreciate the strong vertical variation and weak horizontal variation in potential temperature (Figure 2c). Salinity has similar weak horizontal variability (Figure S2). In Figure 2c, the gray line shows the satellite-derived estimate of ice draft along the calving front from REMA, while the brown area is the bathymetry measured from the downwards ADCP. The warmest SML waters do not extend deep enough to directly access the ice shelf cavity (ignoring the potential for isopycnal deepening and baroclinic flow). At depths with direct access to the ice shelf cavity (below ~300 m), water is near or at the surface freezing point, with a salinity of approximately 34.5. The latitudinal homogeneity is visible, which has aided in the comparison and compilation of data from multiple days. Water sampled in the deepest trough region (at latitude of 68.7°S) was likewise cold and relatively salty without any signature of warmer waters such as MCDW.

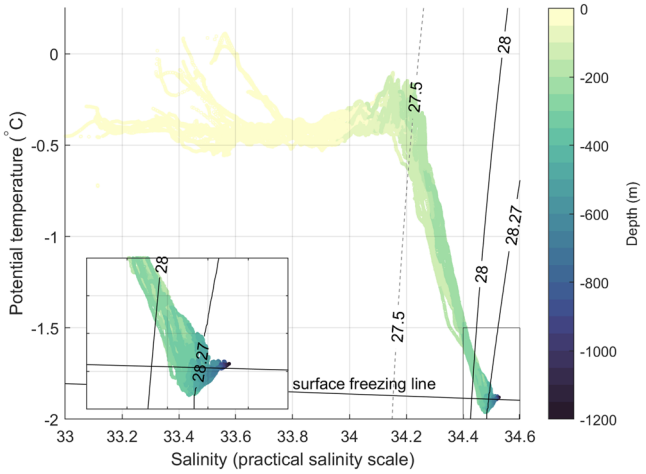

Figure 3. A potential temperature-salinity diagram, colored by depth of observation. The surface freezing point is the solid line, while the inset shows a magnification of the densest observations. The $\sigma_0 = 27.5$ kg m^{-3} potential density anomaly contour delineates surface summer mixed layer water from the Winter Water below; the $\gamma_n = 28.00$ kg m^{-1} and $\gamma_n = 28.27$ kg m^{-1} neutral density anomaly contours are typically used to delineate MCDW (Whitworth et al., 1998; Williams et al., 2010).

A potential temperature-salinity plot, with each sample colored by depth, summarizes this situation (Figure 3). Almost all water that was sampled within 125 m of the surface is warmer than −0.5°C and can be categorized as Antarctic Surface Water (AASW). Mixing with lower salinity surface water, which likely originates from surface melting of nearby icebergs, drives strong salinity variations in this surface water. The potential temperature and salinity at the bottom of the SML (~ −0.4°C, 34.22) allows us to define a threshold potential density anomaly (referenced to the surface), σ_0, which delineates surface waters from the lower WW body. We select a value of $\sigma_0 = 27.5$ kg m^{-3} as an appropriate choice (potential density anomaly plot where SML is clearly delineated by the $\sigma_0 = 27.5$ kg m^{-3} contour is not shown). The bottom of the SML (approximately 125 m) delineates where the effects of summertime wind-driven mixing and surface heating reduce in intensity. From 125 to ~300 m, mixing between the summer waters and the wintertime waters below becomes successively weaker with depth, leading to a transition in properties (especially temperature) to that of the water mass below. Mixing is visible as the diagonal line joining water masses at (−0.4°C, 34.2) to (−1.9°C, 34.5) and represents the remnants of the wintertime mixed layer, otherwise known as WW. The very deepest waters present have temperatures at the surface

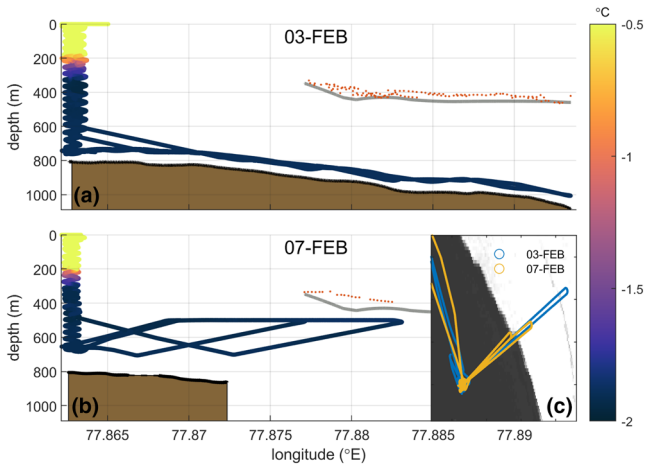

Figure 4. Potential temperature measured during under-ice missions on (a) 3 February and (b) 7 February is shown. (c) Map shows path of each mission below the Sørsdal ice shelf. Orange markers show the inferred ice shelf draft as measured by the upwards-oriented subbottom profiler from the AUV, while the gray line is the draft inferred from the satellite elevation product REMA (Howat et al., 2019).

freezing point (~ -1.89°C; see inset in Figure 3) and with a salinity of 34.52, which corresponds to DSW. There is some water (below surface freezing line in inset of Figure 3) measured at middepths (500 to 600 m), with mean values of $\theta = -1.93$°C and 34.48, which represented a small outflow of Ice Shelf melt Water (ISW). While some water falls between the $\gamma_n = 28.00$ kg m^{-1} and $\gamma_n = 28.27$ kg m^{-1} isopycnal contours, which are typically used to identify MCDW (Whitworth et al., 1998; Williams et al., 2010), the presence of this water at very cold, near-freezing temperatures (-1.63°C to -1.88°C) likely contains no remnants of offshore CDW (Whitworth et al., 1998), and so we stress that this does not represent a true modified CDW.

The two sub-ice shelf missions are shown in Figure 4c, with the 3 February mission traveling some 700 m total beneath the ice shelf. The 7 February mission traveled only 200 m beneath the ice, but did so at a shallower depth, allowing the upper water column to be sampled, and the upwards-oriented subbottom profiler to measure returns from the ice shelf.

The first under-ice mission (Figure 4a) traveled at a constant altitude of 75 m above the seafloor. Water properties were similar to that measured outside the cavity, with cold (~ -1.89°C) and relatively salty (34.5) water extending beneath the ice shelf. The second mission (Figure 2b) dived and returned at a depth of 500 m, sampling similarly cold and relatively salty water. Salinity conditions (Figure S3) on both dives matched the vertical properties observed outside the cavity.

Water velocities within the cavity (Figure 5) were in general weak (<0.2 m s^{-1}). This is particularly true for velocities near the seafloor, which were sampled on the 3 February mission (Figures 5a and 5b). Closer to the ice shelf base, velocities are stronger and flow in a southwest direction as they exit the cavity (Figure 5c). At middepths (600–700 m), there is a weaker return flow toward the northeast present at the ice shelf front. This pattern is consistent with ice shelf cavity outflow dominating the current regime beneath the ice (Figure 5e) and matches ISW measured in the vicinity. As this region has largely unobserved bathymetry, we expect the tidal solution to be poor, and so removal of tidal currents would be largely unreliable. However, on each mission, total time spent beneath the ice was less than 1 hr, and so changes in tidal currents during each mission should be negligible.

3.2. Bathymetry and Seafloor Topography

Subbottom profiler data collected parallel to the calving front of the Sørsdal ice shelf (Figure 6a) reveal irregular, rough seafloor with areas of both limited acoustic penetration with no reflectors and areas with transparent deposits (Figure 6b). Data collected parallel to the calving front show the seafloor slowly deepening from ~400 to ~800 m depth (over 1.8 km), then dropping further into a ~1.2-km-wide, >1,200-m-deep glacial trough (Figure 6b). The offshore-trending glacial trough aligns with the ice flow direction of the ice shelf. The trough is steep-sided and cuts into likely crystalline bedrock with potential mass-wasting deposits lining the sides of the trough. Rising again to 800 m deep, the seafloor undulates for 0.8 km before rising again to 40 m (over 1.1 km) at the opposing end of the calving front. A high-amplitude continuous reflector covers the seafloor with an absence of distinct sedimentary horizons below. Note the ET2205 subbottom profiler aboard the AUV has a maximum penetration of 40 m (in clay); features beneath this depth are likely artifacts or multiples of near-surface reflectors. The glacial trough and rugged terrain resemble glacimarine features observed elsewhere offshore Antarctica (Carson et al., 2017; Lowe & Anderson, 2003; Nitsche et al., 2013; Smith et al., 2009). The subbottom features show a landscape dominated by erosional processes, with crystalline bedrock outcrops interspersed with potentially modern mass-wasting deposits on the flanks.

Side-scan sonar collected beneath (Figures 6c and 6d) and parallel to the calving front (Figure 6e) confirm the rugged seafloor imaged by the subbottom profiler, further reflecting the likely crystalline outcrops of gneiss or paragneiss, as observed in the adjacent Vestfold Hills (O'Brien et al., 2015; Zulbati & Harley, 2007), and reshaped during a past erosion-dominant regime. The steep terrain of the glacial trough inhibited comprehensive side-scan sonar data collection as the AUV was too far from the bottom; however, snippets reveal outcrops and rough topography of seafloor that has undergone reshaping through erosion. A second,

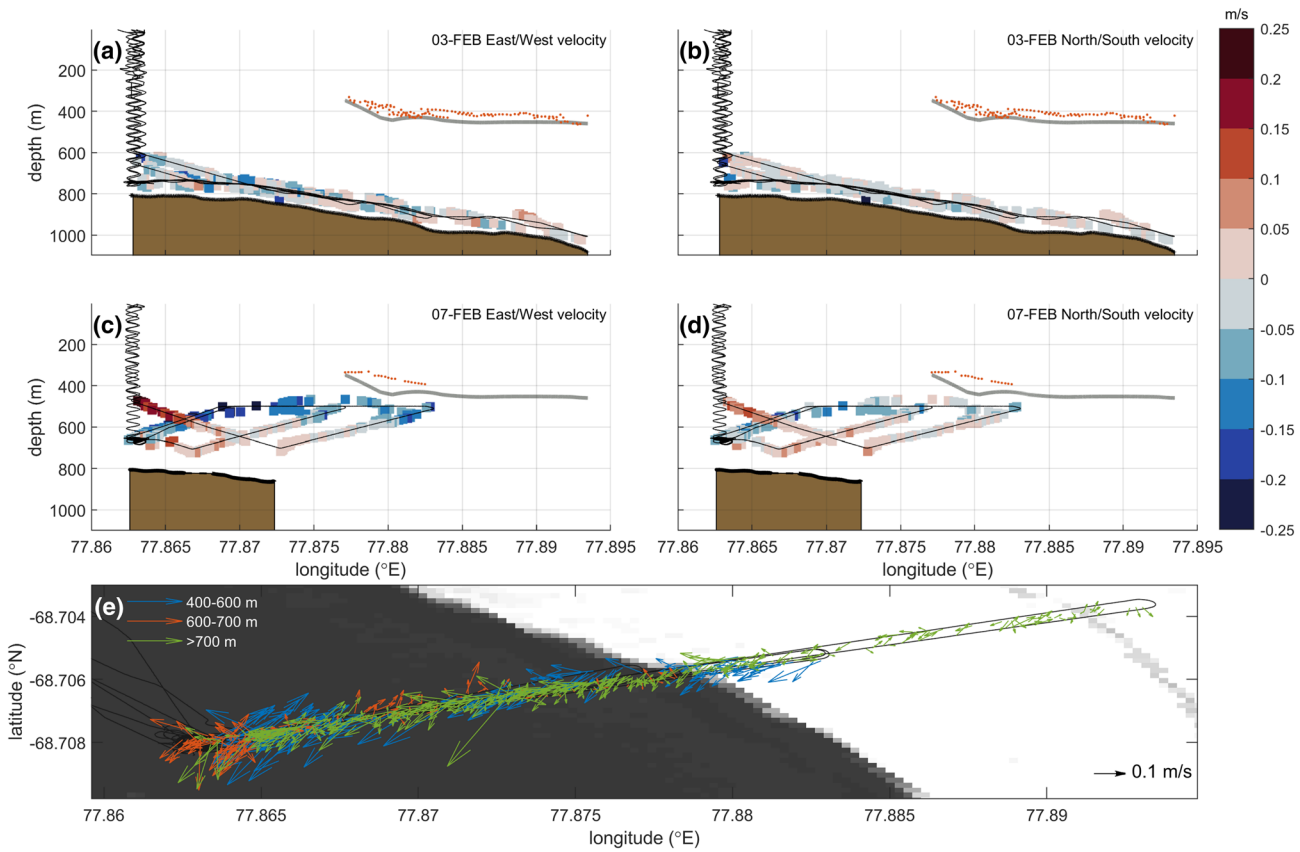

Figure 5. Water velocities measured by onboard ADCP during under-ice missions on (a, b) 3 February and (c, d) 7 February are shown. Panels (a) and (c) show velocities in the east/west direction, corresponding to positive/negative on the color scale, respectively, and panels (b) and (d) show velocities in the north/south direction, corresponding to positive/negative on the color scale, respectively. Orange markers show the inferred ice shelf draft as measured by the upwards-oriented subbottom profiler from the AUV, while the gray line is the draft inferred from the satellite elevation product REMA (Howat et al., 2019). The bottom bathymetry is measured by the onboard ADCP. (e) ADCP currents for both missions. Blue, orange, and green vectors show velocities in the 400–600, 600–700, and >700 m depth range, respectively.

smaller trough and/or sinuous meltwater features in ~800 m water depth have been imaged with side-scan sonar near the southern end of the calving front (Figure 6e). These meltwater features represent channels incised into the bedrock by subglacial meltwater flow, when the Sørsdal Glacier was grounded closer to the continental shelf edge between ~20,000 and ~12,000 ^{14}C yr BP (Anderson et al., 2002; Domack et al., 1998).

Bathymetric and high-resolution side-scan sonar data were not recorded due to complications with the high frequency (520 kHz) array. During the under-ice missions (3 and 7 February), the subbottom profiler was oriented upwards to collect ice topography (see section 3.3).

3.3. Ice Topography

With the AUV tracking the seafloor at a range of 75 m, an expected range of 200–600 m was expected to the basal surface of the ice. A low-frequency subbottom profiler was oriented upward to collect single-point measurements of the ice draft along the AUV route. Extraction of primary ice surface returns provide a measure of the topography, but internal reflections prove difficult to interpret as internal structure. The resulting acoustic lever arm also leads to large sweeps of coverage as the AUV pitches to maintain seafloor tracking. Figure 7 shows the extracted surface returns from the collected subbottom records.

Subbottom profiler data collected beneath the ice shelf provide a measure of ice draft. In the 3 February echogram (Figure 7a), the ice bottom can be seen at ~400 m. In the 7 February echogram (Figure 7b), which tracked closer to the ice shelf base, there are several distinguishable features, including the sea surface return and a basal return. In Figure 7b, a phenomenon is observed in which a strong return begins prior to the expected basal surface, which can be explained as the sonar detecting the vertical face of the ice shelf as

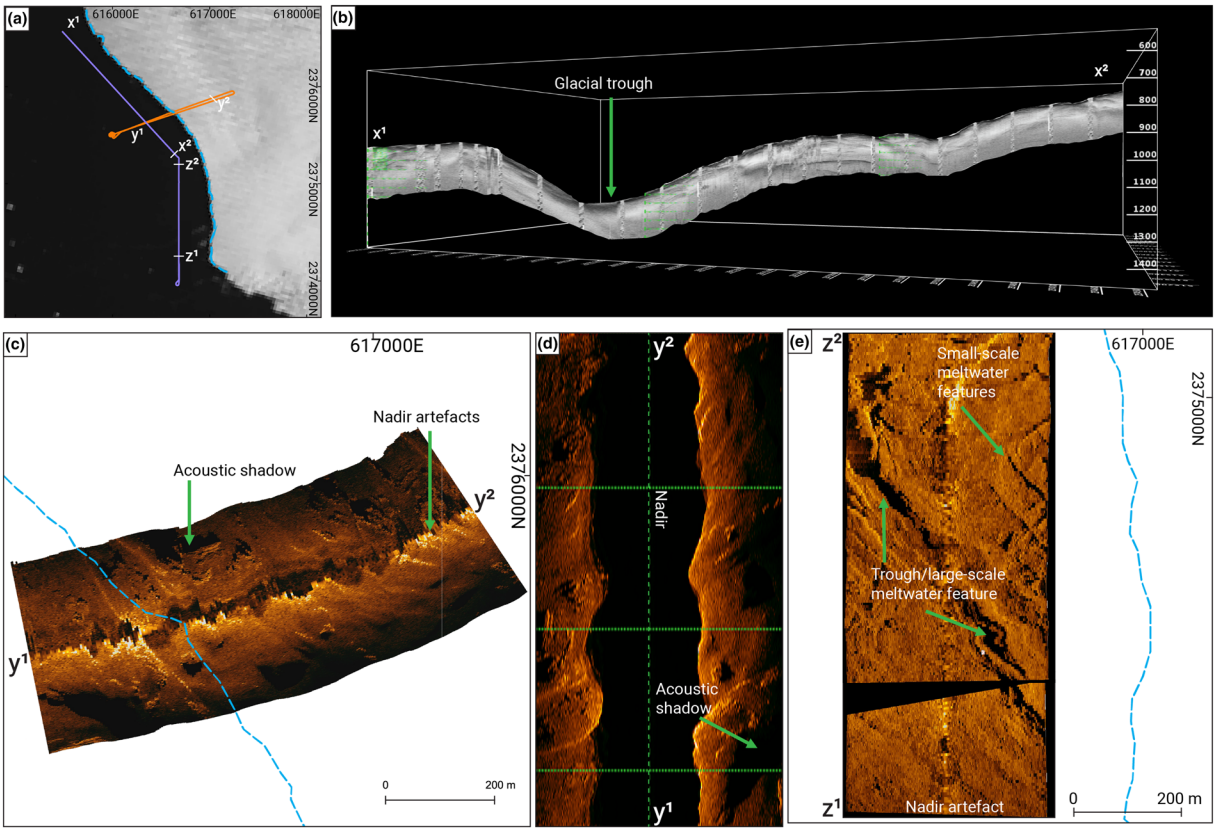

Figure 6. Low-frequency side-scan sonar imagery and subbottom profiler data collected parallel and perpendicular to the calving front reveal rough seafloor terrain and exposed bedrock. (a) Plan view of calving front and survey lines. Blue dashed line shows approximate location of calving front derived from 19 January 2019 Landsat satellite imagery. (b) Subbottom profiler data collected parallel to calving front showing glacial trough (x^1 to x^2 in Figure 5a). Noise columns within the subbottom data are interference from the acoustic modem. (c) Plan view of under-ice mission downward-facing side-scan sonar data showing rugged topography (y^1 to y^2 in Figure 5a). Blue dashed line = calving front. (d) Waterfall view of under-ice mission. Vertical green dashed line is nadir, horizontal green dashed lines are 250 m intervals, and black blank area from nadir to seafloor is water column. (e) Plan view of open-water mission downward-facing side-scan sonar data (z^1 to z^2 in Figure 5a) showing potential past erosional features. Blue dashed line = calving front. Figures in UTM zone 43S, WGS 1984 (EPSG: 32743).

the AUV approaches the cavity. This can be distinguished by a sharp rise in echo intensity when the basal surface enters the sonar view.

The complete echo record for each ping has potential to provide some information about internal structure of the ice, such as fissures and basal crevasses, but is difficult to interpret without reference to known features or a complementary data set.

3.4. Basal Melting Estimates

Oceanographic observations suggest a cold cavity environment conducive to low basal melting. Here, we present results from a numerical ocean model and satellite-inferred estimates, which we compare to direct observations of melt rate taken at two sites on the Sørsdal ice shelf from January 2017 to January 2019.

The estimate of melting from ROMS (Figure 8a) shows highest melting at the rear, deepest part of the cavity, and along the ice front. Refreezing is weak, and the mean melt rate averaged over the whole shelf is 0.5 m yr^{-1}, while modeled melt rates at Sites s02 and s04 (0.24 and 1.1 m yr^{-1}, respectively; see Table 1) are reasonably close to values observed from APRES (s02: 1.6 m yr^{-1}; s04: 2.3 m yr^{-1}). The APRES observations (Figure 8b) show an almost complete absence of seasonal cycle in melt rate, indicating that source waters that drive melting also lack any strong temporal variability. In January to March 2017 and January to March 2018, summertime surface melting flooded the sites. The presence of liquid water inhibited the acquisition of accurate radar returns and prohibits an assessment of the impact of any solar-heat surface water access during summer (e.g., Malyarenko et al., 2019; Stewart et al., 2019).

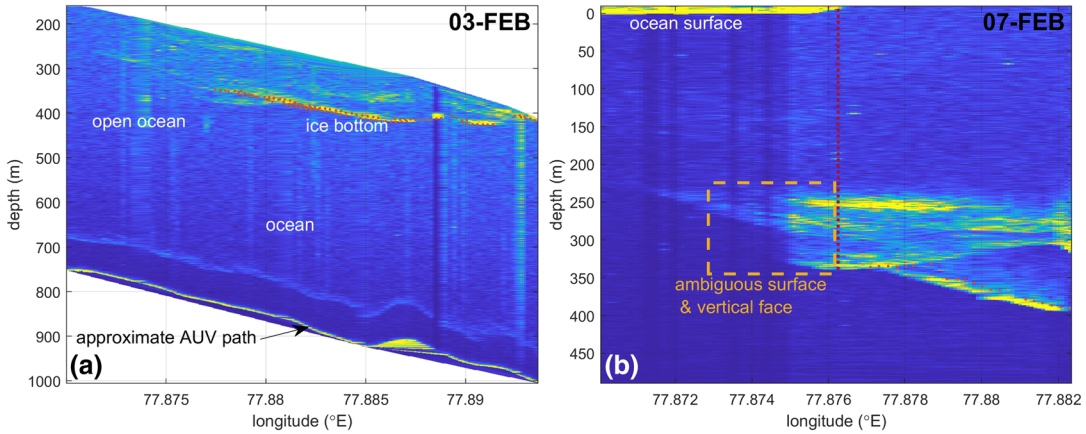

Figure 7. Echograms of subbottom profiler oriented upward into ice. (a) 3 February mission, the longest AUV incursion. (b) 7 February, the shorter incursion but with AUV at closest range to ice. Red dots indicate selected ice edge profile. Echograms are not corrected for pitch/roll of AUV. Note the change of vertical scale.

Satellite-inferred estimates predict basal melting similar to that suggested by the ROMS model (Table 1). The flux gate method using different grounding lines predicts low melt rates that match observed and modeled estimates, but integrated mass loss differs due to the change in area encompassed by the relevant grounding line products.

The estimates of basal mass loss from the volume divergence method (see the supporting information) suggest from 3.0 m yr^{-1} of basal refreezing (with Bedmap2 thickness) to 6.5 m yr^{-1} of basal melting (with REMA thickness). The spatial pattern (Figure S4) is also very different to the spatial pattern of the model results. This may result from uncertainty in the observed ice thickness, which was calculated assuming that the ice is in hydrostatic equilibrium. This assumption breaks down at pinning points on the ice shelf, within an ice thickness of any grounded ice, and in regions with high crevasse density. These conditions cover much of the Sørsdal ice shelf. The surface mass balance used (Arthern et al., 2006) is also likely to overestimate surface mass balance on the ice shelf, as its spatial resolution will miss the high summer surface melt observed on the glacier. The spatial pattern of melt rates from the volume divergence method is additionally affected by

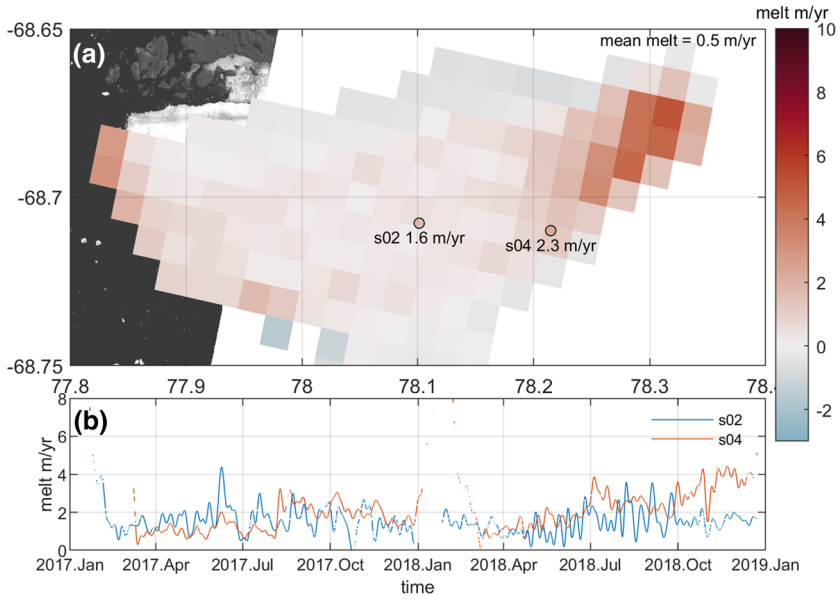

Figure 8. Melt rates of the Sørsdal ice shelf. (a) Numerical ocean model estimates of basal melting are shown in the spatial map. The time-averaged mean melt rate is shown in the top right corner. (b) The time variability in melt rates observed at Sites s02 and s04 (see locations in panel a). The time-averaged melt rates from APRES Sites s02 and s04 are also shown as circles in panel (a), with the circle fill on the same color axis.

Table 1
Area-Averaged Melt Rates for the Sørsdal Ice Shelf Are Summarized for a Variety of Techniques

		Estimate		
	Method type	(m yr^{-1})	(gt yr^{-1})	Notes
Point value	APRES s02	1.6	n/a	Time mean melt rate for the whole deployment after quality control and removal of bad data
	APRES s04	2.3	n/a	Time mean melt rate for the whole deployment after quality control and removal of bad data
	ROMS s02	0.42	n/a	Melt rate from ROMS at APRES Site s02
	ROMS s04	1.1	n/a	Melt rate from ROMS at APRES Site s04
Area average value	ROMS model	0.48	0.068	Area-averaged melting from a numerical model calculated for the last month of integration
	Flux gate (Bedmap2 GL)	0.81	0.018	Thickness inverted from surface elevation from Bedmap2 (Fretwell et al., 2013), grounding line from Bedmap2 (Fretwell et al., 2013), coastline from MEaSUREsv2 (Mouginot et al., 2017), and accumulation from Arthern et al. (2006)
	Flux gate (MEaSUREsv2 GL)	0.56	0.080	Thickness inverted from surface elevation from Bedmap2 (Fretwell et al., 2013), grounding line and coastline from MEaSUREsv2 (Mouginot et al., 2017), and accumulation from Arthern et al. (2006)

the low spatial resolution of the velocity data set, which may explain the different pattern to modeled melt. Consequently, we caution the reader as to the validity of the estimates derived from these inferred methods but report them in the supporting information for completeness. Flux gate estimates are more reliable for spatially averaged melt calculations as the method necessarily ignores any ice dynamics between the two chosen gates (excepting, of course, surface and basal mass change).

4. Discussion

4.1. Weak Basal Melting Beneath the Sørsdal Ice Shelf

The sparseness of observational deployments and the limitations in the satellite-inferred techniques do not allow a full quantification of spatial variability in melt rates. However, a variety of basal melt estimates for the Sørsdal ice shelf all suggest that melting is, on average, weak. Observations from APRES confirm this and show that a seasonal cycle in basal melting is practically nonexistent at the two sampled sites. However, despite the weak observed melting, observations from moorings, ship, and instrumented seals over many years (Guo et al., 2019; Nunes Vaz & Lennon, 1996; Smith et al., 1984; Williams et al., 2010, 2016; Wong et al., 1998) and multiple modeling studies (Galton-Fenzi et al., 2012; Liu et al., 2017, 2018) of the Prydz Bay region have shown that MCDW upwells over the Four Ladies Bank and is present close to the coastline in significant quantity. This MCDW has been shown to (in part) drive melting beneath the AIS (Herraiz-Borreguero et al., 2013; Herraiz-Borreguero et al., 2015) and is known to drive strong melt in other locations around Antarctica (e.g., Walker et al., 2013).

However, our observations over multiple days and multiple deployments find a simple water structure of SML overlying WW, ISW, and DSW with no MCDW present adjacent or beneath the Sørsdal ice shelf. Our observations are limited in spatial extent (the calving front and the near-bottom region beneath the ice shelf) and in temporal extent (scattered sampling between January to February 2019), but given the spatial and temporal homogeneity of our results (e.g., the observed water column structure), this is likely a representative result for austral summer. The lack of seasonal cycle in APRES observations suggests that wintertime conditions, at least within the cavity, are likely similar to summertime. Further ocean observations and moorings are required to confirm this.

Given the large reservoir of ocean heat available near to the ice shelf calving front (<50 km distance to the edge of the Four Ladies Bank), and no obvious bathymetric obstacles to impede MCDW flow, it is curious that the oceanographic environment beneath the Sørsdal ice shelf is cold. One possible reason for the lack of MCDW at the Sørsdal ice shelf is a lack of bathymetric pathwaters for which the water body can flow along toward the calving front. However, given that observations of MCDW in Prydz Bay show that it is a

lower-density water mass compared to other regional water masses (e.g., DSW), it would be unlikely to be the deepest water mass and hence be bathymetrically steered. This seems to be confirmed by the multitude of previous MCDW observations in this region, which show that it is present at a variety of depths but mostly in the upper water column (e.g., Guo et al., 2019). This suggests that bathymetry has a limited impact on restricting MCDW access to the Sørsdal ice shelf.

Possibly, the reason why MCDW is not observed near to the Sørsdal ice shelf is because of the upstream influence of the Barrier and Davis polynyas. Sea ice formation (mostly in the March to October period Tamura et al., 2016) and formation of DSW result in a coastal current that is salty, cold, and dense and likely fills the whole water column in the shallow coastal band along which the ACoC flows. The pooling of DSW in the narrow coastal band in front of the Sørsdal ice shelf could physically inhibit the passage of less dense MCDW. Ocean model results suggest the presence of a cold oceanographic front, which may lead to reduced access of warmer water to the Sørsdal ice shelf (see Figures S5 and S6). The observed water column properties (i.e., a shallow, warm SML above a nearly homogeneous column of WW with DSW at depth) in front of and beneath the Sørsdal ice shelf support the hypothesis that nearby sea ice formation processes reduce access of MCDW. In particular, deep convection in the nearby Barrier and Davis polynyas produces enough dense water to form a higher-density front and a poleward shoaling of isopycnals, meaning that lighter waters (such as MCDW) cannot pass. The fact that APRES observations of melt rate both show little if any seasonal cycle suggests that the oceanographic conditions observed adjacent to and beneath the ice shelf are present all year round.

There is no direct evidence for this "density wall" mechanism; however, several studies support its existence. Williams et al. (2008) show evidence of reduction in MCDW intrusions due to dense water formation near the Mertz Glacier. In summertime, with reduced sea ice formation, degradation of the denser water masses and increased stratification lead to an increased influence of MCDW intrusions. While not indicative of any mechanism, observations in the vicinity of the Terra Nova Bay Polynya and along the coastline of the Western Ross Sea show a water column dominated by a deep layer of dense High Salinity Shelf Water (Budillon & Spezie, 2000; Orsi & Wiederwohl, 2009), without any warmer off-shelf water, despite the presence of MCDW to the east. The route that this MCDW takes as it moves toward the Ross Ice Shelf could also be impacted by the presence of density fronts. Kohut et al. (2013) show the presence of a cold layer in the western Ross Sea, which may act to deepen the MCDW layer and reduce the flow of this MCDW from Joides Trough up and on to Pennell Bank. For Eastern Prydz Bay, Guo et al. (2019) suggest that upwelling of MCDW is due to the buoyancy difference between the denser DSW buoying up the lighter MCDW above. However, closer to the coastline, with a nearby source of DSW (such as the Barrier or Davis polynya) and little destruction of denser waters, there could be enough DSW present that any shoaling of MCDW would be so energetically expensive as to be impossible. While not referred to by name, a "density wall" mechanism has also been hinted at in modeling studies. In future simulations, the erosion of denser water masses and reversal of the poleward density gradient contribute to the flooding of the Filchner-Ronne Ice Shelf cavity with warmer off-shelf waters (Hellmer et al., 2017). Lastly, the "density wall" mechanism is somewhat analogous to the Antarctic Slope Front that forms in some locations along the continental shelf (see review of Thompson et al., 2018). In this case, a combination of on-shelf dense water formation, winds, and Ekman transport lead to the establishment of density gradients that can either prohibit or allow cross-shelf exchange of warmer off-shelf waters.

4.2. Deep Bathymetric Access

Measurements from downwards ADCP show a deep "V-shaped" channel in bathymetry that is aligned with the Sørsdal ice shelf calving front. The deep channel and seafloor features observed by sonar are characteristic of a typical, erosion-dominated glacimarine environment, with bedrock features formed by subglacial meltwater flow, past ice flow, and mass-wasting processes. While further observations are required to assess the along-channel extent and slope, the depth and orientation suggest that it runs underneath the ice shelf, possible as the fjord-like remnant of a past Sørsdal Glacier ice configuration. Indeed, ice draft near the grounding line of the Sørsdal ice shelf, as inverted from surface elevation (Howat et al., 2019), is deep (~1,000–1,500 m). This suggests that bathymetry in the vicinity of the grounding line, which must be at least as deep as the ice draft, is similar to that in the bottom of the channel near the ice front.

The depth of ocean access to the ice shelf cavity is important for controlling the rate of melting. The lowering of the melting point with depth means that for a given ocean temperature, melting is greater at deeper ice

bases. A deeper and wider cavity "mouth" will also increase the net volume of ocean heat present beneath the ice shelf, meaning that cavity processes such as tidally driven mixing and turbulence can transfer more heat to the ice/ocean interface for melting. While AUV observations showed unstratified, cold, and relatively salty WW and DSW beneath the Sørsdal ice shelf (which likely drives the observed low melt rates), this could change in the future.

4.3. Implications for Change

The presence of MCDW has been shown to reduce sea ice production in polynyas through the increased presence of sensible heat (Guo et al., 2019), while the presence of ISW is thought to reduce the production of DSW through a reduction in salt flux into the ocean (e.g., Silvano et al., 2018; Williams et al., 2016). Here, we propose a mechanism whereby a thick, full-depth layer of higher-density water (DSW) blocks access of a lower-density water (MCDW). Oceanography transects support this mechanism in the coastal Prydz Bay region (Guo et al., 2019) by showing a shoaling of the MCDW body progressively southwards.

Projections suggest, however, that reductions in DSW formation and polynya activity could occur in the near future. Such reductions could arise through seasonal changes in wind direction and strengths associated with climate modes such as the Southern Oscillation Index (Kwok & Comiso, 2002), changes in air temperature, which act to "backfill" polynyas (Tamura et al., 2016), or through an increased flux of ISW should circum-Antarctic basal melting continue to increase (Silvano et al., 2018). As a result, a reduction in the density of the ACoC or the DSW body closest to the coast would reduce the "density wall" effect allowing off-shelf MCDW to shoal or upwell. If this occurs, warmer MCDW could gain access to the Sørsdal ice shelf cavity and likely other small ice shelves along this coastline. Given the presence of thick ice and a deep grounding line, the increased ocean heat access to this cavity would have a large impact on ice shelf stability and sea-level contribution.

An alternative source of increased ocean heat to the Sørsdal ice shelf cavity is solar-heated surface SML. The formation of a freshwater wedge at the ice front (e.g., from ice front melting) could lead to the poleward deepening of isopycnals and downwelling of surface waters into the cavity (e.g., Malyarenko et al., 2019). We propose that shallow-ice melting driven by surface waters was not a major source of mass loss at the Sørsdal ice shelf during the sampling period. AUV dives began within 500 m of the ice front, so any downwelling of isopycnals should have been detected, had they been present. APRES data are least reliable during summer (during the maximum period of surface water solar heating), making it inconclusive for this argument. However, strengthening of ice front melting (leading to increased downwelling of isopycnals) or stronger Ekman pumping (from increased easterly winds; e.g., Hattermann et al., 2014) would lead to higher melting of shallower ice. This could lead to the shelf lifting off areas that were previously grounded on pinning points (e.g., Roberts et al., 2017). This reduction in basal and lateral stress will likely alter ice shelf flow and geometry and lead to a change in the calving front position, potentially impacting upon the threshold of passive ice. The impact and timing of any such event on the long-term ice shelf stability is still unknown.

4.4. Recommendations for Antarctic AUV Deployments

Future AUV missions will face the same challenges of navigation and deployment as discussed here. To reach their potential, future AUV missions will ideally be supported with radar surveys of the ice shelf to help reduce uncertainty in ice draft morphology. Caverns and other dramatically undulating surfaces pose a particular problem for navigation based on the tracking of a surface. Acoustic beacons to aid navigation can be installed through boreholes in the ice shelf. Such installations have been made in sea ice (Jalving et al., 2008; Webster et al., 2015) and would provide confidence in both the mapping data and the vehicle's ability to navigate home over long distances, where unaided inertial navigation error can grow to unacceptable levels. It is conceivable that acoustic modem installations through the ice shelf will allow for a degree of command and control of the vehicle for mission updates while deep inside an ice shelf cavity.

It is tempting to apply as many instruments as possible to an AUV in order to get the greatest scientific value from a mission. Interference between acoustic instruments, even at different frequencies, means that pings must be scheduled and prioritized. "Quiet time" is therefore a finite resource and must be split between communication, navigation, and any scientific acoustic system. We suggest that one priority should be the collection of fine-scale ice shelf draft profile data to complement data sets such as ice cores, on-ice seismic, radar, or colocation with surface-visible features such as crevasses. 3-D multibeam data of the ice surface over wide swaths of coverage would significantly aid our understanding of melt and freeze dynamics and

help to parameterize existing glaciological models, key to predicting future sea-level rise contribution. Collecting such data is risky as it requires a proximity to the ice that may leave the vehicle trapped in a crevasse. A phased approach to the ice shelf should involve the use of lower resolution, longer range profiling systems, such as subbottom sonars and Doppler Velocity Logger rangers, to establish a baseline for safe operation. Getting closer to the ice will enable additional measurements to be made, such as temperature and salinity, boundary layer conditions, and turbulent mixing, to further clarify our understanding of basal melt conditions. AUV use should also be complementary with mooring and glider deployment.

5. Conclusion

Ocean heat access to ice shelves has a direct impact on basal melting, which is known to be a major influence on Antarctica's mass loss and sea-level contribution. However, difficulties with observing melting and cavity conditions in situ lead to much uncertainty in Antarctic basal mass loss, especially for smaller ice shelves outside of the research spotlight.

First-time AUV oceanography observations beneath the Sørsdal ice shelf show conditions conducive to low basal melting. The ocean environment beneath this small ice shelf is shown to be a stable cold water cavity, with spatially homogeneous ocean conditions consisting of a warm SML sitting on top of weakly stratified wintertime water masses of WW and DSW all the way to the ocean bottom, with some ISW outflow detected. The depth of the thermocline separating these water bodies is higher than the likely ice shelf calving front draft, meaning that water access to the cavity is likely cold and relatively salty WW and DSW. This excludes the potential for deepening of isopycnals at the ice front and subsequent baroclinic flow, as seen elsewhere. Measurements beneath the ice shelf showed only DSW present near to the cavity floor. We suggest a mechanism whereby dense water produced locally or originating in nearby polynyas prohibits lower-density MCDW from access to the coastline and ice shelf grounding lines.

We also present estimates and observations of basal melting beneath the Sørsdal ice shelf. While the sparseness and relatively short time records do not allow a full characterization, the agreement between different observations, models, and satellite techniques gives high confidence in the assessment of weak basal melting with limited seasonal variability. These records show that melting is on average weak: 1–2 m yr^{-1} from observations and 0.5 m yr^{-1} from ocean model, while satellite-inferred methods vary from 0.6–0.8 to 3–7 m yr^{-1} depending on technique and data sets. In general, inferred basal melt rates agree with the cold ocean cavity environment shown in the AUV observations.

It has been suggested that there could be a potential reduction in dense water formation associated with changes to the strength and size of polynyas or through increased ISW release. If the proposed blocking mechanism is important for reducing access of warmer waters, any reduction in water density along this coastline would reduce shielding from MCDW and likely impact basal melting through increased ocean heat access. Given our measurements of deep bathymetric access to the Sørsdal ice shelf cavity, increased ocean heat supply to this region could see significant changes to basal mass loss and possibly ice shelf stability under a changing climate.

Acknowledgments
Research was supported by the Australian Research Council's Special Research Initiative for Antarctic Gateway Partnership (Project ID SR140300001) and by the Antarctic Climate and Ecosystems Cooperative Research Centre (ACE CRC). Analysis and data handling were achieved with the Antarctic Mapping Toolbox (Greene et al., 2017) and the Climate Data Toolbox for MATLAB (Greene et al., 2019). The authors thank the engineering expertise of I. Bowden-Floyd and K. Zürcher; mechanical and plant crew of the Davis Station Summer Team, in particular D. Smith; the expert boat operators G. Johnstone and M. Davidson; oceanography input from S. Jendersie; and glaciological input from R. Warner.

Data Availability Statement

Data from the 2018/2019 AUV Sørsdal Deployment can be found in the University of Tasmania/Australian Ocean Data Network GeoNetwork portal (https://doi.org/10.25959/5ea8d42a6ed6c); model data can also be accessed through the University of Tasmania/Australian Ocean Data Network GeoNetwork portal (https://doi.org/10.25959/5ea8d68a6ed6d); and data from the 2017–2019 APRES deployments can be found on the Australian Antarctic Data Centre (https://doi.org/10.26179/5cee0d8ec7133).

Conflict of Interest

There is no real or perceived financial conflict of interest for any author.

References

Anderson, J. B., Shipp, S. S., Lowe, A. L., Wellner, J. S., & Mosola, A. B. (2002). The Antarctic Ice Sheet during the Last Glacial Maximum and its subsequent retreat history: A review. *Quaternary Science Reviews*, *21*(1–3), 49–70. https://doi.org/10.1016/S0277-3791(01)00083-X

Arndt, J. E., Schenke, H. W., Jakobsson, M., Nitsche, F. O., Buys, G., Goleby, B., et al. (2013). The International Bathymetric Chart of the Southern Ocean (IBCSO) version 1.0—A new bathymetric compilation covering circum-Antarctic waters. *Geophysical Research Letters*, *40*, 3111–3117. https://doi.org/10.1002/grl.50413

Arneborg, L., Wåhlin, A. K., Björk, G., Liljebladh, B., & Orsi, A. H. (2012). Persistent inflow of warm water onto the central Amundsen shelf. *Nature Geoscience*, *5*(12), 876.

Arthern, R. J., Winebrenner, D. P., & Vaughan, D. G. (2006). Antarctic snow accumulation mapped using polarization of 4.3-cm wavelength microwave emission. *Journal of Geophysical Research*, *111*, D06107. https://doi.org/10.1029/2004JD005667

Brierley, A. S., Fernandes, P. G., Brandon, M. A., Armstrong, F., Millard, N. W., McPhail, S. D., et al. (2002). Antarctic krill under sea ice: Elevated abundance in a narrow band just south of ice edge. *Science*, *295*(5561), 1890–1892. https://doi.org/10.1126/science.1068574

Brito, M. P., Griffiths, G., & Challenor, P. (2010). Risk analysis for autonomous underwater vehicle operations in extreme environments. *Risk Analysis*, *30*(12), 1771–1788. https://doi.org/10.1111/j.1539-6924.2010.01476.x

Budillon, G., & Spezie, G. (2000). Thermohaline structure and variability in the Terra Nova Bay polynya, Ross Sea. *Antarctic Science*, *12*(4), 493–508. https://doi.org/10.1017/S0954102000000572

Carson, C. J., Post, A. L., Smith, J., Walker, G., Waring, P., Bartley, R., & Raymond, B. (2017). The seafloor geomorphology of the Windmill Islands, Wilkes Land, East Antarctica: Evidence of Law Dome ice margin dynamics. *Geomorphology*, *292*, 1–15. https://doi.org/10.1016/j.geomorph.2017.04.031

Church, J. A., Clark, P. U., Cazenave, A., Gregory, J. M., Jevrejeva, S., Levermann, A., et al. (2013). Sea level change. In T. F. Stocker, et al. (Eds.), *Climate change 2013: The physical science basis. Contribution of Working Group I to the Fifth Assessment Report of the Intergovernmental Panel on Climate Change*. Cambridge, United Kingdom and New York, NY, USA: Cambridge University Press.

Collar, P. G., & McPhail, S. D. (1995). Autosub: An autonomous unmanned submersible for ocean data collection. *Electronics & Communication Engineering Journal*, *7*(9), 105–114. https://doi.org/10.1049/ecej:19950305

Cougnon, E. A., Galton-Fenzi, B. K., Meijers, A. J. S., & Legrésy, B. (2013). Modelling inter-annual Dense Shelf Water export in the region of the Mertz Glacier Tongue (1992–2007). *Journal of Geophysical Research: Oceans*, *118*, 5858–5872. https://doi.org/10.1029/2004JD005667

Cougnon, E. A., Galton-Fenzi, B. K., Rintoul, S. R., Legrésy, B., Williams, G. D., Fraser, A. D., & Hunter, J. R. (2017). Regional changes in icescape impact shelf circulation and basal melting. *Geophysical Research Letters*, *44*, 11,519–11,527. https://doi.org/10.1002/2017GL074943

Crees, T., Kaminski, C., Ferguson, J., Laframboise, J. M., Forrest, A., Williams, J., et al. (2010). UNCLOS under ice survey—An historic AUV deployment in the Canadian high Arctic. In *Oceans 2010 MTS/IEEE Seattle* (pp. 1–8). https://doi.org/10.1109/OCEANS.2010.5664438

DeConto, R. M., & Pollard, D. (2016). Contribution of Antarctica to past and future sea-level rise. *Nature*, *531*(7596), 591–597.

Dinniman, M. S., Klinck, J. M., & Smith, W. O. (2007). Influence of sea ice cover and icebergs on circulation and water mass formation in a numerical circulation model of the Ross Sea, Antarctica. *Journal of Geophysical Research*, *112*, C11013. https://doi.org/10.1029/2006JC004036

Domack, E., O'Brien, P., Harris, P., Taylor, F., Quilty, P. G., Santis, L. D., & Raker, B. (1998). Late Quaternary sediment facies in Prydz Bay, East Antarctica and their relationship to glacial advance onto the continental shelf. *Antarctic Science*, *10*(3), 236–246. https://doi.org/10.1017/S0954102098000339

Dutrieux, P., De Rydt, J., Jenkins, A., Holland, P. R., Ha, H. K., Lee, S. H., et al. (2014). Strong sensitivity of Pine Island ice-shelf melting to climatic variability. *Science*, *343*(6167), 174–178. https://doi.org/10.1126/science.1244341

Dutrieux, P., Stewart, C., Jenkins, A., Nicholls, K. W., Corr, H. F. J., Rignot, E., & Steffen, K. (2014). Basal terraces on melting ice shelves. *Geophysical Research Letters*, *41*, 5506–5513. https://doi.org/10.1002/2014GL060618

Edwards, T. L., Brandon, M. A., Durand, G., Edwards, N. R., Golledge, N. R., Holden, P. B., et al. (2019). Revisiting Antarctic ice loss due to marine ice-cliff instability. *Nature*, *566*(7742), 58–64. https://doi.org/10.1038/s41586-019-0901-4

Fretwell, P., Pritchard, H. D., Vaughan, D. G., Bamber, J. L., Barrand, N. E., Bell, R., et al. (2013). Bedmap2: Improved ice bed, surface and thickness datasets for Antarctica. *The Cryosphere*, *7*(1), 375–393. https://doi.org/10.5194/tc-7-375-2013

Fürst, J. J., Durand, G., Gillet-Chaulet, F., Tavard, L., Rankl, M., Braun, M., & Gagliardini, O. (2016). The safety band of Antarctic ice shelves. *Nature Climate Change*, *6*(5), 479–482. https://doi.org/10.1038/nclimate2912

Galton-Fenzi, B. K., Hunter, J. R., Coleman, R., Marsland, S. J., & Warner, R. C. (2012). Modeling the basal melting and marine ice accretion of the Amery Ice Shelf. *Journal of Geophysical Research*, *117*, C09031. https://doi.org/10.1029/2012JC008214

Greene, C. A., Gwyther, D. E., & Blankenship, D. D. (2017). Antarctic Mapping Tools for MATLAB. *Computers and Geosciences*, *104*, 151–157. https://doi.org/10.1016/j.cageo.2016.08.003

Greene, C. A., Thirumalai, K., Kearney, K. A., Delgado, J. M., Schwanghart, W., Wolfenbarger, N. S., et al. (2019). The Climate Data Toolbox for MATLAB. *Geochemistry, Geophysics, Geosystems*, *20*, 3774–3781. https://doi.org/10.1029/2019GC008392

Guo, G., Shi, J., Gao, L., Tamura, T., & Williams, G. D. (2019). Reduced sea ice production due to upwelled oceanic heat flux in Prydz Bay, East Antarctica. *Geophysical Research Letters*, *46*, 4782–4789. https://doi.org/10.1029/2018GL081463

Gwyther, D. E., Cougnon, E. A., Galton-Fenzi, B. K., Roberts, J. L., Hunter, J. R., & Dinniman, M. S. (2016). Modelling the response of ice shelf basal melting to different ocean cavity environmental regimes. *Annals of Glaciology*, *57*(73), 131–141. https://doi.org/10.1017/aog.2016.31

Gwyther, D. E., Galton-Fenzi, B. K., Dinniman, M. S., Roberts, J. L., & Hunter, J. R. (2015). The effect of basal friction on melting and freezing in ice shelf-ocean models. *Ocean Modelling*, *95*, 38–52. https://doi.org/10.1016/j.ocemod.2015.09.004

Gwyther, D. E., Galton-Fenzi, B. K., Hunter, J. R., & Roberts, J. L. (2014). Simulated melt rates for the Totten and Dalton ice shelves. *Ocean Science*, *10*(3), 267–279. https://doi.org/10.5194/os-10-267-2014

Gwyther, D. E., O'Kane, T. J., Galton-Fenzi, B. K., Monselesan, D. P., & Greenbaum, J. S. (2018). Intrinsic processes drive variability in basal melting of the Totten Glacier Ice Shelf. *Nature Communications*, *9*(1), 1–8. https://doi.org/10.1038/s41467-018-05618-2

Hattermann, T., Smedsrud, L. H., Nøst, O. A., Lilly, J. M., & Galton-Fenzi, B. K. (2014). Eddy-resolving simulations of the Fimbul Ice Shelf cavity circulation: Basal melting and exchange with the open ocean. *Ocean Modelling*, *82*, 28–44. https://doi.org/10.1016/j.ocemod.2014.07.004

Hellmer, H. H., Kauker, F., Timmermann, R., & Hattermann, T. (2017). The fate of the southern Weddell Sea continental shelf in a warming climate. *Journal of Climate*, *30*(12), 4337–4350. https://doi.org/10.1175/JCLI-D-16-0420.1

Herraiz-Borreguero, L., Allison, I., Craven, M., Nicholls, K. W., & Rosenberg, M. A. (2013). Ice shelf/ocean interactions under the Amery Ice Shelf: Seasonal variability and its effect on marine ice formation. *Journal of Geophysical Research: Oceans*, *118*, 7117–7131. https://doi.org/10.1002/2013JC009158

Herraiz-Borreguero, L., Coleman, R., Allison, I., Rintoul, S. R., Craven, M., & Williams, G. D. (2015). Circulation of modified Circumpolar Deep Water and basal melt beneath the Amery Ice Shelf, East Antarctica. *Journal of Geophysical Research: Oceans*, *120*, 3098–3112. https://doi.org/10.1002/2015JC010697

Holland, P. R., Jenkins, A., & Holland, D. M. (2008). The response of ice shelf basal melting to variations in ocean temperature. *Journal of Climate*, *21*(11), 2558–2572. https://doi.org/10.1175/2007JCLI1909.1

Howat, I. M., Porter, C., Smith, B. E., Noh, M.-J., & Morin, P. (2019). The Reference Elevation Model of Antarctica. *The Cryosphere*, *13*(2), 665–674. https://doi.org/10.5194/tc-13-665-2019

Hui, F., Ci, T., Cheng, X., Scambos, T. A., Liu, Y., Zhang, Y., et al. (2014). Mapping blue-ice areas in Antarctica using ETM+ and MODIS data. *Annals of Glaciology*, *55*(66), 129–137. https://doi.org/10.3189/2014AoG66A069

Jalving, B., Faugstadmo, J. E., Vestgärd, K., Hegrenaes, O., Engelhardtsen, O., & Hyland, B. (2008). Payload sensors, navigation and risk reduction for AUV under ice surveys. In *2008 IEEE/OES autonomous underwater vehicles* (pp. 1–8). https://doi.org/10.1109/AUV.2008.5290525

Jendersie, S., Williams, M. J. M., Langhorne, P. J., & Robertson, R. (2018). The density-driven winter intensification of the Ross Sea circulation. *Journal of Geophysical Research: Oceans*, *123*, 7702–7724. https://doi.org/10.1002/2015JC010697

Jenkins, A., Nicholls, K. W., & Corr, H. F. J. (2010). Observation and parameterization of ablation at the base of Ronne Ice Shelf, Antarctica. *Journal of Physical Oceanography*, *40*(10), 2298–2312. https://doi.org/10.1175/2010JPO4317.1

Jenkins, A., Shoosmith, D., Dutrieux, P., Jacobs, S., Kim, T. W., Lee, S. H., et al. (2018). West Antarctic Ice Sheet retreat in the Amundsen Sea driven by decadal oceanic variability. *Nature Geoscience*, *11*(10), 733–738. https://doi.org/10.1038/s41561-018-0207-4

Kimura, S., Jenkins, A., Dutrieux, P., Forryan, A., Naveira Garabato, A. C., & Firing, Y. (2016). Ocean mixing beneath Pine Island Glacier ice shelf, West Antarctica. *Journal of Geophysical Research: Oceans*, *121*, 8496–8510. https://doi.org/10.1002/2016JC012149

King, M. A., Coleman, R., Freemantle, A. J., Fricker, H. A., Hurd, R. S., Legrésy, B., et al. (2009). A 4-decade record of elevation change of the Amery Ice Shelf, East Antarctica. *Journal of Geophysical Research*, *114*, F01010. https://doi.org/10.1029/2008JF001094

Kohut, J., Hunter, E., & Huber, B. (2013). Small-scale variability of the cross-shelf flow over the outer shelf of the Ross Sea. *Journal of Geophysical Research: Oceans*, *118*, 1863–1876. https://doi.org/10.1002/jgrc.20090

Kwok, R., & Comiso, J. C. (2002). Southern Ocean climate and sea ice anomalies associated with the Southern Oscillation. *Journal of Climate*, *15*(5), 487–501. https://doi.org/10.1175/1520-0442(2002)015h0487:SOCASIi2.0.CO;2

Liu, Y., Moore, J. C., Cheng, X., Gladstone, R. M., Bassis, J. N., Liu, H., et al. (2015). Ocean-driven thinning enhances iceberg calving and retreat of Antarctic ice shelves. *Proceedings of the National Academy of Sciences*, *112*(11), 3263–3268. https://doi.org/10.1073/pnas.1415137112

Liu, C., Wang, Z., Cheng, C., Wu, Y., Xia, R., Li, B., & Li, X. (2018). On the modified circumpolar deep water upwelling over the Four Ladies Bank in Prydz Bay, East Antarctica. *Journal of Geophysical Research: Oceans*, *123*, 7819–7838. https://doi.org/10.1029/2018JC014026

Liu, C., Wang, Z., Cheng, C., Xia, R., Li, B., & Xie, Z. (2017). Modeling modified Circumpolar Deep Water intrusions onto the Prydz Bay continental shelf, East Antarctica. *Journal of Geophysical Research: Oceans*, *122*, 5198–5217. https://doi.org/10.1002/2016JC012336

Lowe, A. L., & Anderson, J. B. (2003). Evidence for abundant subglacial meltwater beneath the paleo-ice sheet in Pine Island Bay, Antarctica. *Journal of Glaciology*, *49*, 125–138. https://doi.org/10.3189/172756503781830971

Malyarenko, A., Robinson, N. J., Williams, M. J. M., & Langhorne, P. J. (2019). A wedge mechanism for summer surface water inflow into the Ross Ice Shelf cavity. *Journal of Geophysical Research: Oceans*, *124*, 1196–1214. https://doi.org/10.1029/2018JC014594

Massom, R. A., Harris, P. T., Michael, K. J., & Potter, M. J. (1998). The distribution and formative processes of latent-heat polynyas in East Antarctica. *Annals of Glaciology*, *27*, 420–426.

Mouginot, J., Rignot, E., Scheuchl, B., & Millan, R. (2017). Comprehensive annual ice sheet velocity mapping using Landsat-8, Sentinel-1, and RADARSAT-2 data. *Remote Sensing*, *9*(4), 364. https://doi.org/10.3390/rs9040364

Mueller, R. D., Padman, L., Dinniman, M. S., Erofeeva, S. Y., Fricker, H. A., & King, M. A. (2012). Impact of tide-topography interactions on basal melting of Larsen C Ice Shelf, Antarctica. *Journal of Geophysical Research*, *117*, C05005. https://doi.org/10.1029/2011JC007263

Nicholls, K. W., Abrahamsen, E. P., Buck, J. J. H., Dodd, P. A., Goldblatt, C., Griffiths, G., et al. (2006). Measurements beneath an Antarctic ice shelf using an autonomous underwater vehicle. *Geophysical Research Letters*, *33*, L08612. https://doi.org/10.1029/2006GL025998

Nicholls, K. W., Abrahamsen, E. P., Heywood, K. J., Stansfield, K., Nicholls, K. W., Abrahamsen, E. P., & Heywood, K. J. (2008). High-latitude oceanography using the Autosub autonomous underwater vehicle. *Limnology and Oceanography*, *53*(5), 2309–2320.

Nicholls, K. W., Corr, H. F., Stewart, C. L., Lok, L. B., Brennan, P. V., & Vaughan, D. G. (2015). A ground-based radar for measuring vertical strain rates and time-varying basal melt rates in ice sheets and shelves. *Journal of Glaciology*, *61*(230), 1079–1087.

Nicholls, K. W., Padman, L., Schröder, M., Woodgate, R. A., Jenkins, A., & Østerhus, S. (2003). Water mass modification over the continental shelf north of Ronne Ice Shelf, Antarctica. *Journal of Geophysical Research*, *108*(8), 3260. https://doi.org/10.1029/2002JC001713

Nitsche, F. O., Gohl, K., Larter, R. D., Hillenbrand, C. D., Kuhn, G., Smith, J. A., et al. (2013). Paleo ice flow and subglacial meltwater dynamics in Pine Island Bay, West Antarctica. *The Cryosphere*, *7*, 249–262. https://doi.org/10.5194/tc-7-249-2013

Nunes Vaz, R. A., & Lennon, G. W. (1996). Physical oceanography of the Prydz Bay region of Antarctic waters. *Deep Sea Research Part I: Oceanographic Research Papers*, *43*(5), 603–641. https://doi.org/10.1016/0967-0637(96)00028-3

O'Brien, P. E., Smith, J., Stark, J. S., Johnstone, G., Riddle, M., & Franklin, D. (2015). Submarine geomorphology and sea floor processes along the coast of Vestfold Hills, East Antarctica, from multibeam bathymetry and video data. *Antarctic Science*, *27(6)*, 566–586. https://doi.org/10.1017/S0954102015000371

Orsi, A. H., & Wiederwohl, C. L. (2009). A recount of Ross Sea waters. *Deep Sea Research Part II: Topical Studies in Oceanography*, *56*(13–14), 778–795. https://doi.org/10.1016/j.dsr2.2008.10.033

Paolo, F. S., Padman, L., Fricker, H. A., Adusumilli, S., Howard, S., & Siegfried, M. R. (2018). Response of Pacific-sector Antarctic ice shelves to the El Niño/Southern Oscillation. *Nature Geoscience*, *11*(2), 121–126. https://doi.org/10.1038/s41561-017-0033-0

Rignot, E., Mouginot, J., Scheuchl, B., van den Broeke, M., van Wessem, M. J., & Morlighem, M. (2019). Four decades of Antarctic Ice Sheet mass balance from 1979–2017. *Proceedings of the National Academy of Sciences*, *116*(4), 1095–1103. https://doi.org/10.1073/pnas.1812883116

Roberts, J. L., Galton-Fenzi, B. K., Paolo, F. S., Donnelly, C., Gwyther, D. E., Padman, L., et al. (2017). Ocean forced variability of Totten Glacier mass loss. *Geological Society, London, Special Publications*, *461*, 175–186.

Sasgen, I., Konrad, H., Helm, V., & Grosfeld, K. (2019). High-resolution mass trends of the Antarctic Ice Sheet through a spectral combination of satellite gravimetry and radar altimetry observations. *Remote Sensing*, *11*(2), 144. https://doi.org/10.3390/rs11020144

Schröder, L., Horwath, M., Dietrich, R., Helm, V., van den Broeke, M. R., & Ligtenberg, S. R. M. (2019). Four decades of Antarctic surface elevation changes from multi-mission satellite altimetry. *The Cryosphere*, *13*(2), 427–449. https://doi.org/10.5194/tc-13-427-2019

Silvano, A., Rintoul, S. R., Peña-Molino, B., Hobbs, W. R., Van Wijk, E., Aoki, S., et al. (2018). Freshening by glacial meltwater enhances melting of ice shelves and reduces formation of Antarctic Bottom Water. *Science Advances*, *4*(4), 1–12. https://doi.org/10.1126/sciadv.aap9467

Smith, J. A., Hillenbrand, C.-D., Larter, R. D., Graham, A. G. C., & Kuhn, G. (2009). The sediment infill of subglacial meltwater channels on the West Antarctic continental shelf. *Quaternary Research*, *71*(2), 190–200. https://doi.org/10.1016/j.yqres.2008.11.005

Smith, N. R., Zhaoqian, D., Kerry, K. R., & Wright, S. (1984). Water masses and circulation in the region of Prydz Bay, Antarctica. *Deep Sea Research Part A. Oceanographic Research Papers*, *31*(9), 1121–1147. https://doi.org/10.1016/0198-0149(84)90016-5

St-Laurent, P., Klinck, J. M., & Dinniman, M. S. (2013). On the role of coastal troughs in the circulation of warm Circumpolar Deep Water on Antarctic Shelves. *Journal of Physical Oceanography*, *43*(1), 51–64. https://doi.org/10.1175/JPO-D-11-0237.1

Stewart, C. L., Christoffersen, P., Nicholls, K. W., Williams, M. J. M., & Dowdeswell, J. A. (2019). Basal melting of Ross Ice Shelf from solar heat absorption in an ice-front polynya. *Nature Geoscience*, *1*. https://doi.org/10.1038/s41561-019-0356-0

Tamura, T., Ohshima, K. I., Fraser, A. D., & Williams, G. D. (2016). Sea ice production variability in Antarctic coastal polynyas. *Journal of Geophysical Research: Oceans*, *121*, 2967–2979. https://doi.org/10.1002/2015JC011537

Thompson, A. F., Stewart, A. L., Spence, P., & Heywood, K. J. (2018). The Antarctic Slope Current in a changing climate. *Reviews of Geophysics*, *56*, 741–770. https://doi.org/10.1029/2018RG000624

Walker, D. P., Jenkins, A., Assmann, K. M., Shoosmith, D. R., & Brandon, M. A. (2013). Oceanographic observations at the shelf break of the Amundsen Sea, Antarctica. *Journal of Geophysical Research: Oceans*, *118*, 2906–2918. https://doi.org/10.1002/jgrc.20212

Webster, S. E., Freitag, L. E., Lee, C. M., & Gobat, J. I. (2015). Towards real-time under-ice acoustic navigation at mesoscale ranges. In *2015 IEEE International Conference on Robotics and Automation (ICRA)* (pp. 537–544).

Whitworth, T. III., Orsi, A. H., Kim, S.-J., Nowlin Jr, W. D., & Locarnini, R. A. (1998). Water masses and mixing near the Antarctic Slope Front. In *Ocean, ice, and atmosphere: Interactions at the Antarctic continental margin* (Vol. 75, pp. 1–27). American Geophysical Union.

Williams, G. D., Bindoff, N. L., Marsland, S. J., & Rintoul, S. R. (2008). Formation and export of Dense Shelf Water from the Adélie Depression, East Antarctica. *Journal of Geophysical Research*, *113*, C04039. https://doi.org/10.1029/2007JC004346

Williams, G. D., Herraiz-Borreguero, L., Roquet, F., Tamura, T., Ohshima, K. I., Fukamachi, Y., et al. (2016). The suppression of Antarctic bottom water formation by melting ice shelves in Prydz Bay. *Nature Communications*, *7*(6), 1–9. https://doi.org/10.1038/ncomms12577

Williams, G. D., Maksym, T., Wilkinson, J., Kunz, C., Murphy, C., Kimball, P., & Singh, H. (2015). Thick and deformed Antarctic sea ice mapped with autonomous underwater vehicles. *Nature Geoscience*, *8*(1), 61–67. https://doi.org/10.1038/ngeo2299

Williams, G. D., Nicol, S., Aoki, S., Meijers, A. J. S., Bindoff, N. L., Iijima, Y., et al. (2010). Surface oceanography of BROKE-West, along the Antarctic margin of the south-west Indian Ocean (30–80° E). *Deep Sea Research Part II: Topical Studies in Oceanography*, *57*(9–10), 738–757. https://doi.org/10.1016/j.dsr2.2009.04.020

Wong, A. P. S., Bindoff, N. L., & Forbes, A. (1998). Ocean-ice shelf interaction and possible bottom water formation in Prydz Bay, Antarctica. In *Ocean, ice, and atmosphere: Interactions at the Antarctic continenal margin* (Vol. 75, pp. 173–187). https://doi.org/10.1029/ar075p0173

Wynn, R. B., Huvenne, V. A. I., Bas, T. P. L., Murton, B. J., Connelly, D. P., Bett, B. J., et al. (2014). Autonomous Underwater Vehicles (AUVs): Their past, present and future contributions to the advancement of marine geoscience. *Marine Geology*, *352*, 451–468. 50th Anniversary Special Issue. https://doi.org/10.1016/j.margeo.2014.03.012

Zulbati, F., & Harley, S. L. (2007). Late Archaean granulite facies metamorphism in the Vestfold Hills, East Antarctica. *Lithos*, *93(1–2)*, 39–67. https://doi.org/10.1016/j.lithos.2006.04.004